OPEN ACCESS
Journal of Innovative Optical Health Sciences
Vol. 17, No. 2 (2024) 2350024 (15 pages)

DOI: 10.1142/S1793545823500244

World Scientific
www.worldscientific.com

MMAE-loaded PLGA nanomedicine with improved biosafety to achieve efficient antitumor treatment

Changqiang Xie[*,†], Yan Wang[*,†], Zhenzhen Cai[*,†], Jianghai Du[*,†], Zhengyu Chen[*,†], Junjie Wang[‡,§,¶] and Xingzhou Peng[*,†,‖]

[*]*State Key Laboratory of Digital Medical Engineering*
School of Biomedical Engineering
Hainan University, Haikou 570228, P. R. China

[†]*Key Laboratory of Biomedical Engineering of Hainan Province*
One Health Institute, Hainan University
Haikou 570228, P. R. China

[‡]*Key Laboratory of Hainan Trauma and Disaster Rescue*
The First Affiliated Hospital of Hainan Medical University
Hainan Medical University, Haikou 571199, P. R. China

[§]*Engineering Research Center for Hainan Bio-Smart Materials and Bio-Medical Devices, Key Laboratory of Emergency and Trauma Ministry of Education, Key Laboratory of Hainan Functional Materials and Molecular Imaging, College of Emergency and Trauma*
Hainan Medical University, Haikou 571199, P. R. China
[¶]*jjwanghnmc@163.com*
[‖]*pengxzh@hainanu.edu.cn*

Received 10 June 2023
Accepted 18 August 2023
Published 7 October 2023

Monomethyl auristatin E (MMAE) is a derivative of the marine peptide Dolastatin 10, which has therapeutic effects against various cancers according to its antimitotic activity in multiple clinical trials. The antibody drug conjugate (ADC) of MMAE is currently used in clinical practice. However, the safety issues of MMAE-based ADC, such as high drug toxicity and poor bioavailability, still exist when using it for anticancer therapy. A sustained release of drug delivery approach should be used to reduce toxicity and achieve sufficient anticancer effects. Herein, PLGA-b-PEG_{2000} with excellent biocompatibility and slow degradation ability was adopted to construct MMAE-loaded nanoparticles for safe and effective chemotherapy. The sustained release effect and the immunogenic cell death (ICD) effect of PLGA-MMAE nanoparticles were assessed by *in vitro* experiments. The PLGA-MMAE nanoparticles

[¶,‖]Corresponding authors.

effectively accumulated in the tumor through the enhanced permeability and retention (EPR) effect, inducing cell apoptosis and causing a certain degree of immune response. The sustained drug release of PLGA-MMAE improved the bioavailability and effectively reduced the toxicity and development of the tumor compared to the effect of free MMAE or ADC. Overall, this study provides a safe and effective chemotherapeutic approach, as well as a simple and effective synthetic process for MMAE-based nanoparticles, improving their therapeutic efficacy and safety.

Keywords: Monomethyl auristatin E; poly (lactic-co-glycolic acid) nanoparticles; sustained release; chemotherapy; immunogenic cell death.

1. Introduction

The different living environments of marine and terrestrial organisms have led to the unique structural characteristics of the biodiversity and peptide secondary metabolites in marine organisms.[1,2] Recently, extensive efforts have been directed on the use of marine peptides for antitumor research.[3] Various studies have shown that marine peptides inhibit tumor cell proliferation and metastasis, as well as induce tumor cell apoptosis. Some types of peptides derived from marine organisms, such as sea anemone toxin,[4] dehydrodidemnin B,[5] halichondrin B,[6] and kahalalide F,[7] have been proven to possess broad biological activity and pharmacological properties.

Dolastatin 10, a marine peptide, isolated from the mollusk Dolabella Auricularia, achieved a breakthrough in clinical practice. The active ingredient of Dolastatin 10 is composed of three unique amino acid residues, which effectively induce tumor cell apoptosis even at concentration of nanomolar scale.[7] MMAE, a derivative of Dolastatin 10,[8] is a small molecule with a similar effect as that of typical antitumor medicines (e.g., vinblastine, vincristine, vinorelbine, and paclitaxel)[9–12] since it inhibits the polymerization of microtubules and blocks cell division or apoptosis in the G2/M phase.[13,14] Although MMAE demonstrates a 100-1000 times higher antitumor efficacy than doxorubicin,[15] its high cytotoxicity prevents its use as a stand-alone drug, severely hindering its clinical application. Currently, the administration of antibody drug conjugates (ADCs) offers a promising approach to target specific antibodies on the surface of tumor cells, facilitating the effective delivery of MMAE into the tumor. This targeted delivery mechanism enhances the accumulation of MMAE specifically into the tumor, while minimizing its effect on normal tissues, thereby reducing the side effects associated with systemic cytotoxicity.[16] So far, the US Food and Drug Administration (FDA) has approved five ADCs related to MMAE, namely Adcetrics, Polivy, Padcev, Vidiximab, and Tivdak.[17–20] These drugs have been applied to treat various diseases, such as Hodgkin's lymphoma, diffuse large B-cell lymphoma, advanced urothelial carcinoma, triple HER2-positive gastric cancer, and recurrent or metastatic cervical cancer.[21,22]

Despite the significant achievements of MMAE-based ADCs in clinical trials, their use is still problematic. One issue is represented by the off-target effects that may arise during the systemic administration.[23] On the one hand, the instability of the linker connecting the antibody and the drug can lead to a premature drug release before reaching the intended target. On the other hand, normal tissue cells may inadvertently capture ADCs due to their low expression of receptors or nonspecific uptake, causing unintended toxicity.[24] These phenomena contribute to the premature release of MMAE, leading to adverse effects such as peripheral neuropathy and neutropenia, among other toxic side effects.[25]

Several studies speculate that when the transfer efficiency through blood circulation is 50%, merely 1.56% of the ADCs may reach the desired tumor.[26] The actual amount of ADC reaching solid tumors during a clinical treatment is less than 0.1% of the total administered dose, resulting in the requirement of multiple treatment cycles of ADC chemotherapy, which, unfortunately, brings significant toxicity and adverse side effects.[26,27] Therefore, the dosage should be clinically controlled due to concern of systemic toxicity. Besides, the antibody moieties of

MMAE-ADCs typically come from exogenous antibodies, which may cause immune reactions and immunogenicity issues. This may lead to problems such as allergic reactions and rapid drug clearance, thereby affecting the therapeutic effect of ADCs.[24,28]

Poly(lactic-co-glycolic acid) (PLGA) is a polymer material approved by the FDA for clinical treatment,[29] which can be degraded into metabolized lactate and glycolic acid by hydrolysis *in vivo*.[30] PLGA is typically used as a matrix to construct nanocarriers with a sustained and effective release of proteins or peptides, antibiotics and chemicals due to its biocompatibility and biodegradability *in vivo*.[31,32] In addition, the drug loaded in nanocarriers is effectively protected from the enzymatic degradation, resulting in good stability and efficient delivery.[33] The delivery system of PLGA nanoparticles (NPs) may improve the solubility, stability, and bioavailability of a drug, reducing the dosage and toxicity compared with traditional drug delivery routes, such as tablets, capsules and gels. Moreover, the EPR effect can be used to increase the local accumulation in the tumor site.[34] Polyethylene glycol (PEG) modification is another commonly adopted strategy to bypass the capture by the reticuloendothelial system (RES), thus enhancing the active targeting of NPs.[35]

Here, we incorporated a polyethylene glycol segment (PEG_{2000}) into the PLGA and created PLGA-MMAE nanomedicine through a hydrophobic self-assemble process. PEGlyated NPs extended the blood circulation time, targeted murine breast carcinoma (4T1) tumor through the EPR effect and performed a sustained release of MMAE molecules during the degradation of PLGA NPs over a longer period of time, thus inhibiting tumor growth (Scheme 1). During blood circulation, the bust

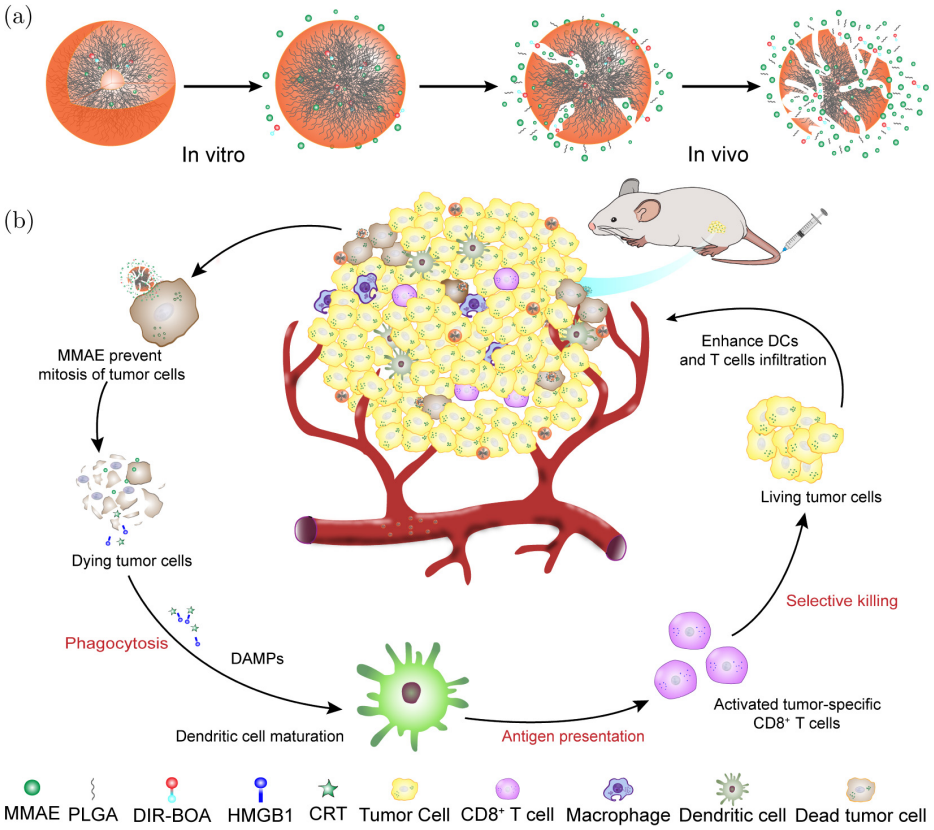

Scheme 1. Schematic illustration of the mechanism of action of PLGA-MMAE NPs for a sustained release of MMAE. (a) When PLGA-MMAE NPs are used *in vivo*, their ester bonds are gradually broken down, resulting in the reduction of the molecular weight and mass loss of the polymer chains. Since the NPs degraded slowly, MMAE and DiR-BOA are released into the tumor microenvironment. (b) After intravenous injection, PLGA-MMAE NPs accumulate in the tumor through the EPR effect. PLGA-MMAE NPs sustainably release MMAE to induce apoptosis of tumor cells, then the tumor cells are involved in the ICD process with the release or exposure of damage-associated molecular patterns (DAMPs), thereby activating the maturation and antigen presentation of DCs, subsequently activating cytotoxic T cells (CTLs) and B cells, forming a specific antitumor immune response.

release of MMAE was prevented because MMAE was distributed into the interior of the PLGA NPs. In addition, the sustained release of therapeutics avoided the acute cytotoxicity caused by a high local concentration and improved the bioavailability of drugs. Finally, PLGA-MMAE NPs contributed to the infiltration of T cells and dendritic cells (DCs) through the ICD effect, induced effective antitumor immune responses, and inhibited the growth of the tumor.

2. Materials and Methods

2.1. *Reagents*

L-(-)-Lactide and 1,4-Dioxane-2,5-dione were purchased from Energy-chemical (Anqing, China). Ethyl ether, dichloromethane, chloroform, and dimethylformamide were obtained from Xilong Scientific Co., Ltd. (Shenzhen, China). Trifluoroacetic acid was purchased from Aladdin (Shanghai, China). Polyethylene glycol $_{2000}$ was purchased from Macklin Biochemical Technology Co., Ltd. (Shenzhen, China). Acetonitrile was purchased from Fisher Chemical (Pennsylvania, USA). Tin (II)2-ethylhexanoate was purchased from Sigma-Aldrich (St. Louis, Missouri, USA). High mobility group box 1 (HMGB1) antibody was purchased from Bioss (Beijing, China). Calreticulin (CRT) antibody was purchased from Affinity Biologicals Inc (Ontario, Canada). The terminal deoxynucleotidyl transferase-mediated dUTP-biotin nick end labeling (TUNEL) assay kit was purchased from Beyotime (Nanjing, China).

2.2. *Synthesis of PLGA-b-PEG$_{2000}$ and PLGA-MMAE NPs*

The synthesis of PLGA-b-PEG$_{2000}$ was performed according to a previous report.[36] Briefly,bib1,4-Dioxane-2,5-dione, L-(-)-Lactide, Tin (II)2-ethylhexanoate and PEG$_{2000}$ were mixed in the Schlenk reactor under the condition of nitrogen protection and let them react at room temperature for 24 h. Pure PLGA-b-PEG$_{2000}$ was obtained through precipitation. The self-assembled PLGA-MMAE NPs were prepared under ultrasonic conditions.

2.3. *Characterization of physicochemical properties of PLGA-MMAE*

The DLS size and zeta potential of the samples were measured by Malvern pro (Malvern Panalytical, Zetasizer Advance Series-Pro). The stability of PLGA-MMAE was determined, by resuspending the NPs in PBS at 4°C and 37°C. The particle size was monitored with a fixed time interval.

2.4. *Loading efficiency and in vitro release of PLGA-MMAE NPs*

The content of MMAE was determined by high performance liquid chromatography (HPLC; Waters e2965). The chromatographic conditions were the following: Accucore^{TM} C18 column, detection wavelength 220 nm, mobile phase of acetonitrile and ultrapure water (0.1% trifluoroacetic acid), sample volume 10 μL. The PLGA-MMAE NPs were dissolved by acetonitrile dissolution, and MMAE was released into the solvent. The solubility of PLGA-b-PEG$_{2000}$ in acetonitrile was reduced by adding 15% ultrapure water. PLGA was removed by filtration using a 0.22 μm filter membrane, and the filtrate was diluted 50 times before loading for detection.

The release of MMAE from PLGA-MMAE was performed by dialysis in PBS at 37°C. A total of 0.5 mL PLGA-MMAE was added into a dialysis bag (molecular weight cut-off: 2000), then quickly immersed in 10 mL PBS, at 37°C under gentle shaking speed and the dialysate was changed at fixed time intervals. The amount of MMAE released at each time point was measured by HPLC after the dialysate was lyophilized and eluted with acetonitrile (0.1% trifluoroacetic acid). Three parallel samples were set up in each group.

2.5. *Determination of cell viability and analysis of combination effect*

The cytotoxicity of PLGA-MMAE was assessed and the IC50 was calculated by the CCK-8 assay. An amount of 8000 cells was seeded in a 96-well plate and incubated for 24 h at 37°C and 5% CO_2. The free MMAE and PLGA-MMAE at different concentrations (0.01, 0.1, 1, 10, 100, and 1000 nM) were incubated with 4T1 cells for 24 h. After incubation, the cells were incubated with complete culture medium containing 10% CCK-8 reagent at 37°C for 1 h. The absorbance at 450 nm was measured using a microplate reader (MOLECULAR DEVICES, Spectra Max Id3) to determine the percentage of cell viability.

The effect of PLGA-MMAE incubation at different times on 4T1 cell viability was assessed by seeding 6000 cells in a 96-well plate, which were incubated for 12 h at 37°C and 5% CO_2. The free MMAE (10 nM) and PLGA-MMAE (10 nM) were incubated with 4T1 cells for 0.5, 6, 12, 24, 48, and 72 h. After incubation, the cells were incubated with complete culture medium containing 10% CCK-8 reagent at 37°C for 1 h. The absorbance at 450 nm was measured using a microplate reader (MOLECULAR DEVICES, Spectra Max Id3) to determine the percentage of cell viability.

2.6. *Uptake of PLGA-MMAE nanoparticles by 4T1 cells*

A total of 1×10^6 4T1 cells were seeded into each well of an 8-well chambered culture slide (Thermo Fisher Scientific, CN). The cells were incubated with PLGA-MMAE@DiR-BOA nanoparticles (DiR-BOA: 15 μM) at 37°C for 0 h, 0.5 h, 2 h, 4 h, 8 h, and 12 h. Subsequently, the cells were fixed with 4% paraformaldehyde for 25 min and stained with Hoechst 33342 solution in the dark for 15 min. Finally, the 4T1 cells were visualized using a confocal laser scanning microscope (CLSM) equipped with Hoechst 33342 (405 nm) and Cy5.5 (640 nm) lasers (Olympus FV 3000, Tokyo, Japan).

2.7. *ICD induced expression in vitro*

The PLGA-MMAE and free MMAE (MMAE concentration: 10 nM) were incubated with 4T1 cells for 24 h. The CRT and HMGB1 antibodies were added according to the immunofluorescence staining procedure. Alexa Fluor® 488 and Alexa Fluor® 594 secondary antibodies were used to treat the cells at 37°C for 2 h. DAPI was used to stain the nuclei for 10 min at room temperature. The degree of ICD was evaluated by fluorescence images. (Olympus FV 3000, Tokyo, Japan).

2.8. *In vivo distribution of PLGA-MMAE*

The DiR-BOA loaded NPs (PLGA-MMAE@DiR-BOA, DiR-BOA: 50 μM) were intravenously injected into 4T1 tumor-bearing mice. The fluorescence imaging was recorded at desired times (0, 6, 12, 24, and 48 h) and obtained using a NIR-I *in vivo* imaging system (NIRVana HS, China).

2.9. *In vivo antitumor effect of PLGA-MMAE*

Female Balb/c mice (6–8 weeks old) were purchased from Hunan SJA Laboratory Animal Co., Ltd (Changsha, Hunan, China). One-hundred μL 4T1 cell suspensions (1×10^7 cells/mL) were subcutaneously injected into the flank of Balb/c mice. When the tumors reached 50 mm^3 (8–10 days), the mice were randomly divided into four groups ($n = 4$ per group). Saline, PLGA, free MMAE or PLGA-MMAE NPs at a dose of 4 mg/kg (MMAE concentration) were intravenously injected into the mice. Mouse weight and tumor volume were measured every day, and the tumor volume was calculated using the formula $0.5 \times L \times W^2$. After 15 days of treatment, the blood, tumor, and main organs (heart, liver, spleen, lung, and kidney) of all mice were collected, and hematoxylin-eosin (H&E) staining was performed to evaluate the abnormal morphology of the organs. Alanine aminotransferase (ALT), aspartate aminotransferase (AST), and blood urea nitrogen (BUN) levels were measured to evaluate the function of liver and kidney.

2.10. *TUNEL staining*

Tumors were fixed in 4% paraformaldehyde at 4°C for 12 h and then dehydrated using a 30% sucrose solution. The tumors were then frozen in OCT compound (Sakura, Torrance, CA, USA) and sliced (Leica, Germany). Next, they were stained with DAPI and TUNEL dyes, and data were collected using a confocal fluorescence microscope (Olympus FV 3000, Tokyo, Japan). The images were analyzed by ImageJ software.

2.11. *Statistical analysis*

Statistical analysis was performed using GraphPad Prism software. One-way analysis of variance (ANOVA) followed by Tukey's multiple comparisons test was performed in the comparison of three or more groups. Experimental results were expressed as mean ± standard deviation (SD) from at least three independent trials. A value of $P < 0.05$ was considered statistically significant.

3. Results

3.1. *Preparation and characterization of PLGA-MMAE NPs*

The preparation of PLGA-MMAE nanomedicine was carried out using a thin film rehydration process. Firstly, MMAE and PLGA-b-PEG_{2000} were distributed into a thin membrane, ultrapure water was added dropwise under ultrasonic conditions to form the NPs through hydrophobic interaction with a high loading efficiency of MMAE in PLGA-MMAE NPs (78.7%) (Figs. 1(a) and S1). Subsequently, the size of the NPs was characterized around 168 nm, which is beneficial to the biodistribution in the tumor *via* EPR effect[37] (Fig. 1(b)), and can be applied to the subsequent *in vivo* experiments. Then the size and zeta potential of PLGA-MMAE were 168 nm and −4 mV, respectively. In addition, the size of PLGA-MMAE remained the same (approximately 168 ± 5 nm) for 72 h regardless of the storage at 4°C or 37°C, showing good stability in water solution (Fig. 1(c)). *In vitro* release experiments showed that PLGA-MMAE performed a sustained release of MMAE molecules in PBS (pH 7.4, 37°C). HPLC quantitative analysis revealed that the release of PLGA-MMAE only reached approximately 50% within 3 days (Fig. 1(d)). In summary, PLGA-MMAE NPs were obtained with a high MMAE loading yield and stability. Moreover, these stable NPs with a particle size of approximately 168 nm remained intact without releasing MMAE during blood circulation. After the accumulation in the tumor through EPR, PLGA-MMAE continuously released MMAE, which might result in an improved chemotherapeutic effect.

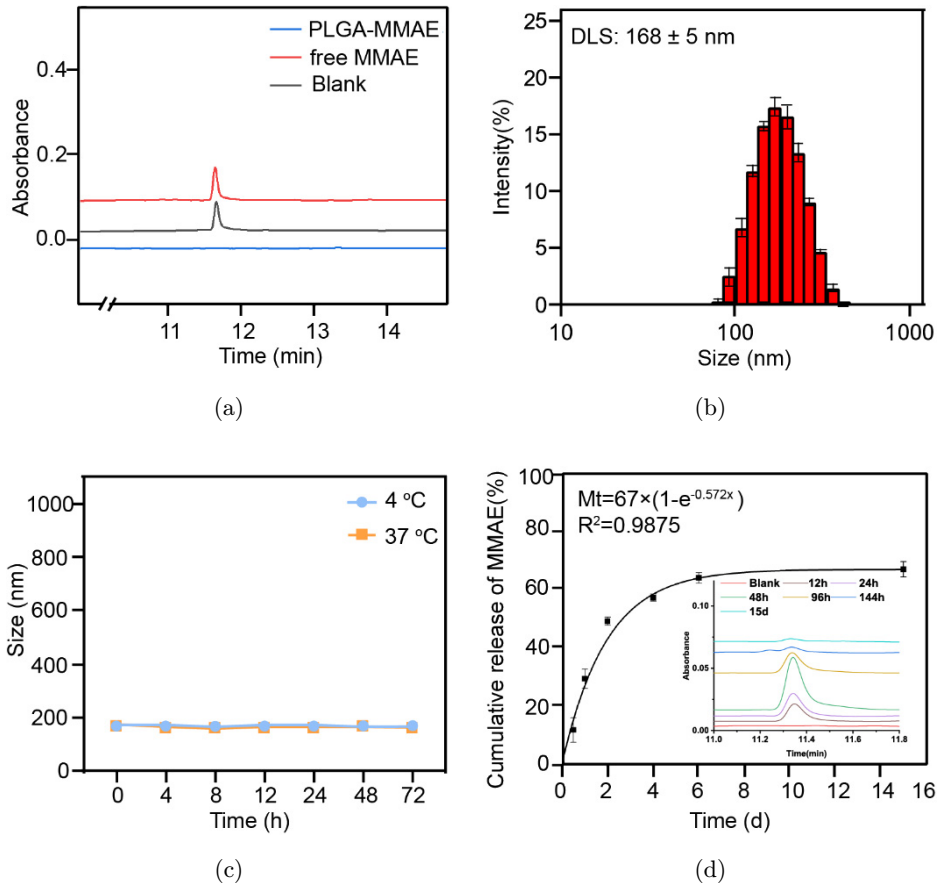

Fig. 1. Characterization of PLGA-MMAE NPs. (a) Determination of the encapsulation efficiency of MMAE in PLGA-MMAE NPs by HPLC. (b) Size distribution of PLGA-MMAE NPs. Results are presented as mean ± SD, $n = 3$. (c) Stability of PLGA-MMAE NPs in water at 4°C or 37°C. Results are presented as mean ± SD, $n = 3$. Determination of the encapsulation efficiency of MMAE in PLGA-MMAE NPs by HPLC. (d) Release profile of MMAE from PLGA-MMAE NPs, demonstrating their release behavior. Results are presented as mean ± SD, $n = 3$.

3.2. *Cell uptake and cytotoxicity of PLGA-MMAE NPs on tumor cells*

To evaluate the time-dependent cellular uptake of PLGA-MMAE nanoparticles, 4T1 cells were utilized. Moreover, PLGA-MMAE@DiR-BOA nanocomplexes were used to allow accurate monitoring. 4T1 cells were treated with PLGA-MMAE@DiR-BOA NPs (MMAE: 10 nM; DiR-BOA: 15 μM) at 37°C, and a substantial and evident cell uptake was observed. The DiR-BOA fluorescence signal of the NPs within the cells gradually increased in a time-dependent manner (Fig. 2(a)). The cytotoxicity of PLGA-MMAE nanomedicines was evaluated *in vitro* by CCK-8 assay, in comparison with the free MMAE after incubation for 24 h at different concentrations. Cell viability after the treatment with PLGA-MMAE nanomedicines was higher than that of free MMAE at all concentrations. The free MMAE had an IC50 value of 10 nM, while the IC50 of PLGA-MMAE was 430 nM at 24 h, indicating that the toxicity of the PLGA-MMAE was much lower than the free MMAE (Fig. 2(b)). In addition, consistent results were obtained in both MC38 and Panc02-H7 cells (Fig. S2). Further research on the cytotoxic effect of different incubation times (MMAE: 10 nM) revealed that the cell inhibition rate of PLGA-MMAE is gradually comparable to that of the free MMAE over time. These results indicated that PLGA-MMAE NPs had the ability to perform a sustained release of MMAE and exerted cytotoxic effects on 4T1 cells in a dose-dependent and time-dependent manner (Fig. 2(c)).

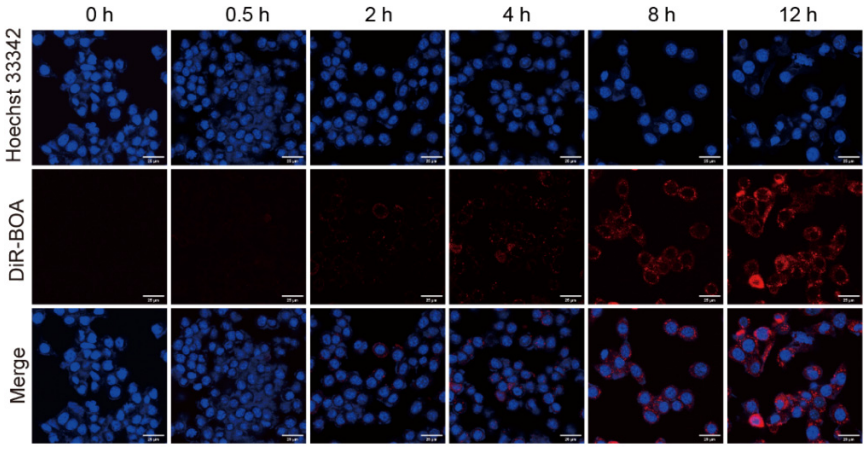

(a)

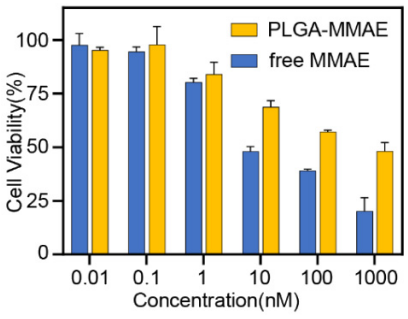

(b)

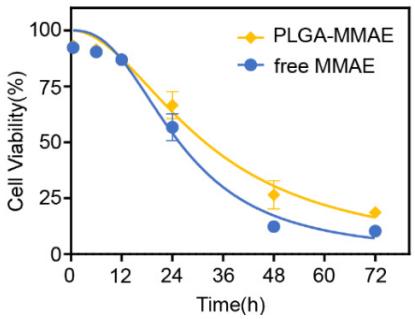

(c)

Fig. 2. (Color online) Cell uptake and cytotoxicity of PLGA-MMAE NPs on tumor cells. (a) Cell uptake of PLGA-MMAE NPs by 4T1 cells. Scale bar: 25 μm. (b) Cell viability of 4T1 tumor cells treated with PLGA-MMAE and free MMAE at different concentrations (0–1000 nM) for 24 h evaluated by CCK-8 assay. Results are presented as mean ± SD, $n = 5$. (c) 4T1 cell viability after co-incubation with PLGA-MMAE or free MMAE for 3, 6, 12, 24, 48, and 72 h. Cell viability was measured by CCK-8 assay. Results are presented as mean ± SD, $n = 5$. (d) Immunofluorescence staining images of 4T1 cells treated with free MMAE (10 nM) and PLGA-MMAE (10 nM) for 24 h. Nuclei were stained with DAPI (blue), CRT (green) and (e) HMGB1 (red). Scale bar: 20 μm.

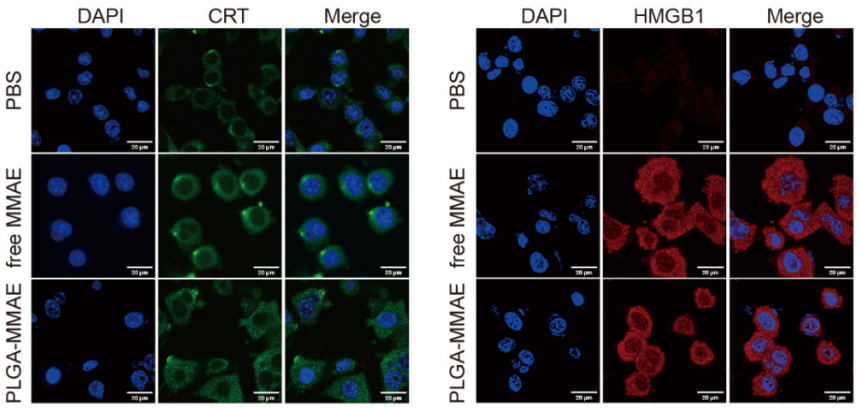

(d) (e)

Fig. 2. (*Continued*)

ICD is a distinct type of functional response that involves the induction of organelles and cellular stress, and results in cell death accompanied by exposure to massive DAMPs, active secretion, or passive release,[38] stimulating DCs to take up and present antigens, as well as fostering DC activation and maturation.[39,40] ICD caused by MMAE can benefit the activation of the subsequent antitumor immune responses. The ICD caused by MMAE nanomedicine was assessed by the immunofluorescence staining of CRT and HMGB1. Due to the permeabilization of the cell samples, a faint CRT signal can be also observed in PBS group.[38,41] Both MMAE and PLGA-MMAE demonstrated more obvious CRT signals and the release of the HMGB1 protein, as compared to after the group treated with PBS (Figs. 2(d) and 2(e)). However, the CRT and HMGB1 fluorescence signals induced by the PLGA-MMAE NPs were weaker than those of the free MMAE, mainly due to the less MMAE content resulting from the sustained release of the PLGA-MMAE. These results suggested that PLGA-MMAE effectively triggered ICD *in vitro*, exerting an immune stimulation *in vivo*.

3.3. *Antitumor effect and safety of PLGA-MMAE NPs in breast tumor-bearing mice*

Encouraged by the outstanding outcomes *in vitro*, the antitumor effect of PLGA-MMAE was further carried out *in vivo*. First, the *in vivo* distribution of PLGA-MMAE in breast cancer bearing mice was investigated by NIR fluorescence. When the tumor volume reached 50 mm^3, PLGA-MMAE@DiR-BOA NPs (MMAE: 4 mg/kg, DiR-BOA: 50 μM) were intravenously injected. PLGA-MMAE@DiR-BOA NPs could efficiently extravasate the cargo DiR-BOA from blood vessels to diffuse through the extracellular matrix, and penetrate and be retained in the tumor site.[42] Real-time images revealed strong fluorescence signals in the tumor area, indicating the successful accumulation of the NPs in the tumor tissue (Fig. 3). The fluorescence signal in the tumor was further enhanced in a time-dependent manner, indicating that PLGA-MMAE effectively remained in the tumor for up to 48 h, releasing DiR-BOA and MMAE in a sustained manner, which enhanced the therapeutic effect. In summary, these results

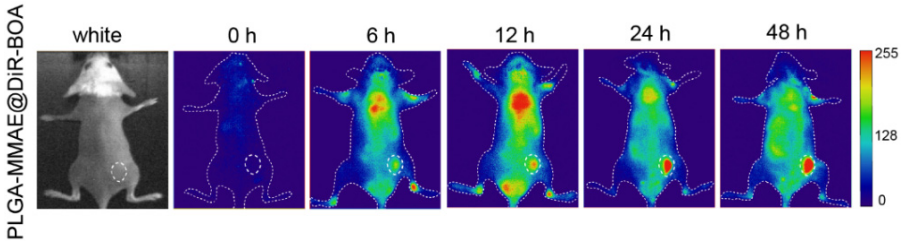

Fig. 3. NIR imaging of the *in vivo* distribution of PLGA-MMAE. NIR-I images of 4T1 tumor-bearing mice treated with PLGA-MMAE@DiR-BOA.

demonstrated the potential of PLGA-MMAE NPs for the targeted delivery into the tumor through the EPR effect.

When the average tumor volume of each group of mice reached 50 mm^3, the mice were randomly divided into four groups: PBS, PLGA, free MMAE and PLGA-MMAE (MMAE: 4 mg/kg). After intravenous injection, the biophysical conditions of the mice in each group (weight, tumor volume, and survival status) were recorded. During the treatment, the body weight of mice treated with PLGA-MMAE NPs began to return to normal levels by the 10th day after the treatment, while the mice in the free MMAE group were all dead on the 4th day due to the severe systemic toxicity of free MMAE (Figs. 4(a) and 4(b)). The tumor volume of the mice in the PLGA-MMAE group was reduced more than 5 times in comparison with the tumor in the PBS or PLGA group (Figs. 4(c) and 4(d)). These results suggested that PLGA-MMAE not

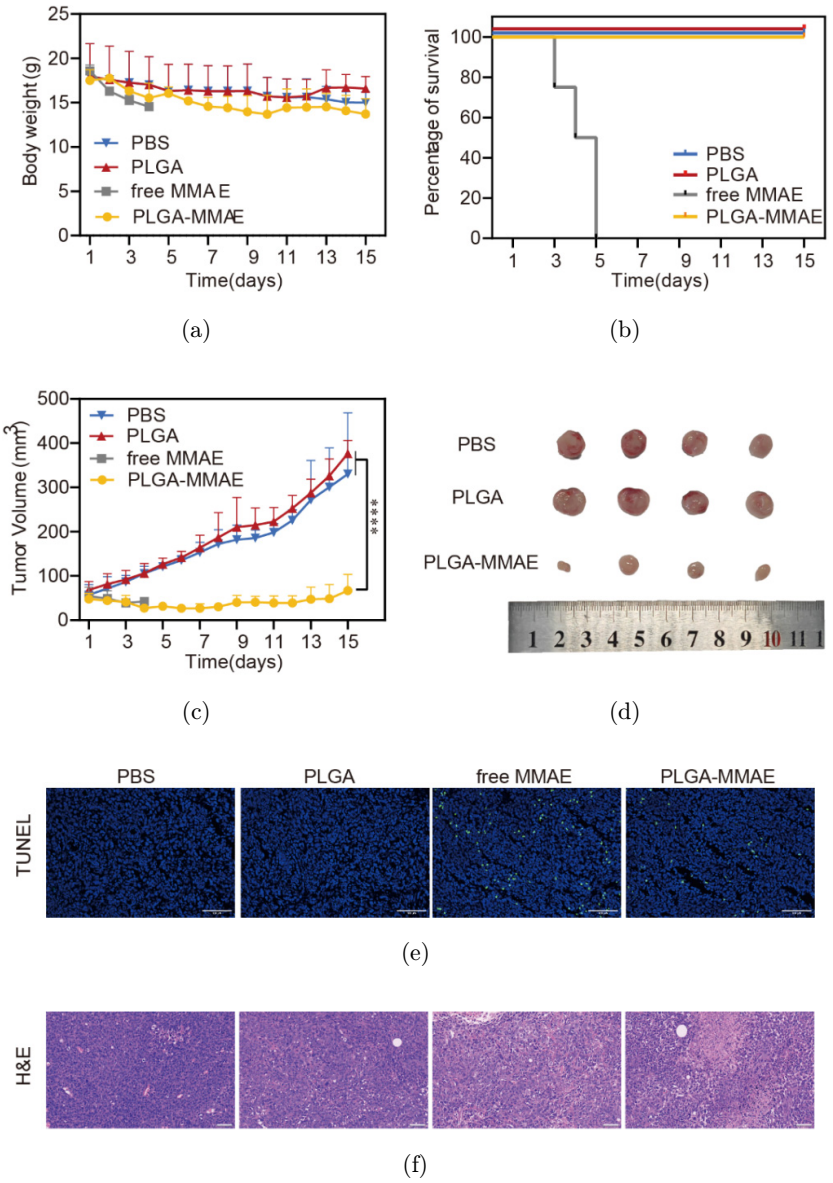

Fig. 4. Antitumor effect of PLGA-MMAE NPs in breast cancer-bearing mice. (a) Body weight changes of mice during the treatment period. (b) Survival curves of mice after the treatment. (c) Tumor growth curves of 4T1 tumor-bearing mice treated with normal saline solution, PLGA, free MMAE or PLGA-MMAE NPs after a single injection into the tail vein. (d) Tumor volumes of 4T1 tumor-bearing mice at the end of the treatment. (e) TUNEL staining of the tumor of mice treated with different regimens. Scale bar: 100 μm. (f) H&E staining of the tumor of mice treated with different regimens. Scale bar: 50 μm. Results are presented as mean $\pm$ SD ($n = 4$). $^{****}P < 0.001$, $^{***}P < 0.001$, $^{**}P < 0.01$, $^{*}P < 0.05$.

only effectively improved the survival time of tumor-bearing mice, but also significantly inhibited tumor growth. At the end of treatment (on the 15th day), the tumor of each group was harvested and subjected to H&E and TUNEL staining. A more intense fluorescence signal was detected in the group treated with PLGA-MMAE and MMAE compared to other treatments, indicating an increase in apoptotic tumor cells, as shown in Fig. 4(e). Moreover, the H&E staining also confirmed the apoptosis, showing significant damage in the tumor of both PLGA-MMAE and free MMAE groups (Fig. 4(f)).

After 15 days of treatment, the physiologic and biochemical indexes of blood and H&E staining of the main organs (heart, liver, spleen, lung, and kidney) were measured to evaluate the biosafety of PLGA-MMAE NPs *in vivo*. The sections of the organs of the free MMAE group showed tissue loosening and increased intercellular space, especially the liver, which showed evident structural abnormalities (black arrows). These results indicated the severe systemic toxicity of free MMAE (Fig. 5(a)).

In addition, the hematological parameters related to liver function such as ALT and AST

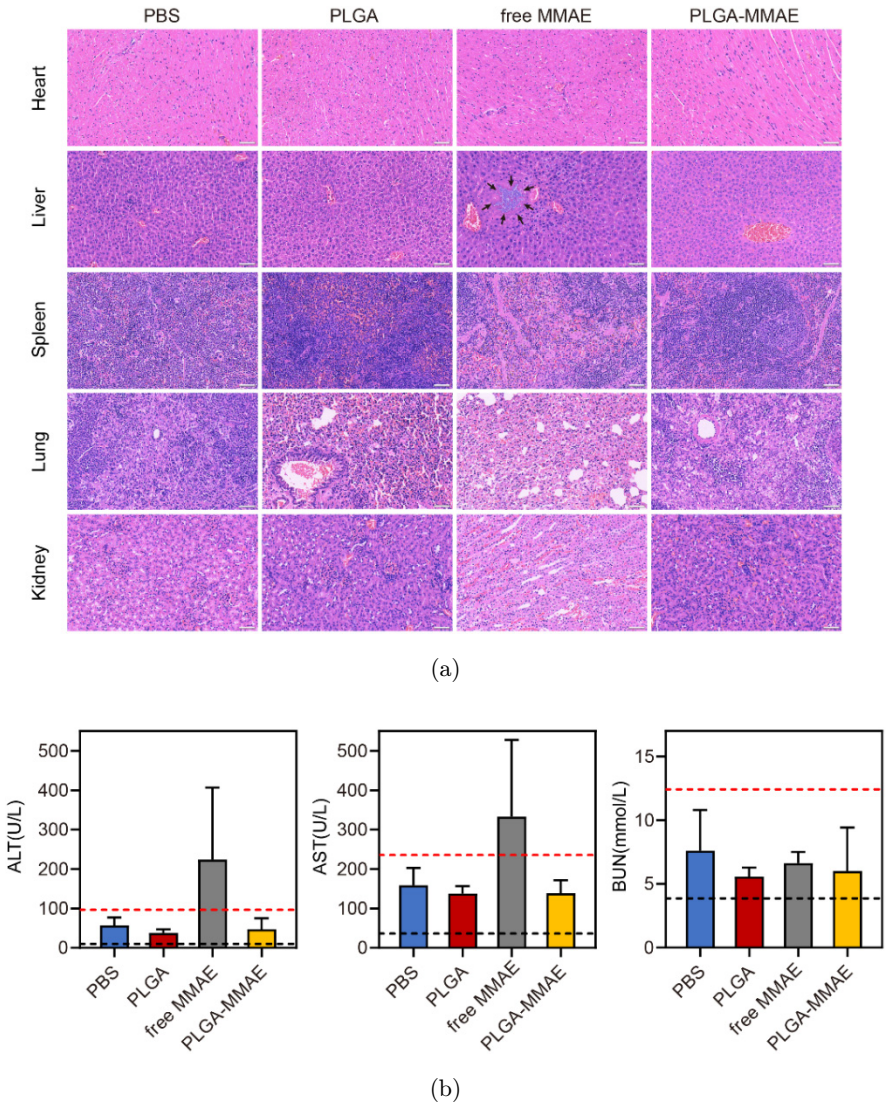

Fig. 5. Biosafety of PLGA-MMAE NPs in breast tumor-bearing mice. (a) The tumor and organ samples used for H&E staining were collected after 15 days of treatment with PBS, PLGA NPs and PLGA-MMAE NPs, free MMAE only treated for 5 days. Scale bar: 50 μm. (b) Hematological parameters of the mice treated with PBS, PLGA NPs and PLGA-MMAE NPs (treated for 15 days), free MMAE only treated for 5 days before mouse death. The structural abnormalities in the liver are pointed by black arrows. Results are presented as mean $\pm$ SD, $n = 4$.

significantly changed in the free MMAE group but remained within a normal range in the PLGA-MMAE group and were similar to those in the PBS group (Fig. 5(b)). These results indicated that MMAE-related toxicity in the PLGA-MMAE group was significantly reduced. In conclusion, the research results indicated that PLGA NPs modified were of good biocompatibility.

3.4. *Tumor immune mechanism induced by PLGA-MMAE NPs*

The flow cytometry analysis of the immune cell infiltration in the tumor after treatment was performed to investigate the detailed antitumor mechanism of PLGA-MMAE NPs (Figs. 6 and S3, S4).

However, due to the toxic effects of the drug, the mice in the free MMAE group died before the end of the treatment and were not subjected to flow cytometry analysis. The mature DCs in the tumor were labeled by CD80 and CD86 antibodies. The percentage of mature DC in the PLGA-MMAE-treated group increased from 6.18 % (PBS group) to 39.56 % (Figs. 6(a) and 6(c)). This result suggested that PLGA-MMAE might cause a higher degree of ICD, release more tumor-associated antigens (TAA), and induce a stronger immune response.[43] In addition, an increased proportion of $CD8^+$ T cells in the tumor (5.7-fold increase compared with the PBS group) was detected in the PLGA-MMAE-treated group (Figs. 6(b) and 6(d)). These results suggested that PLGA-MMAE NPs induced tumor cell apoptosis, promoted DC maturation and T cell infiltration through the sustained release of MMAE in the tumor, generating an immune response against the tumor *in vivo*.

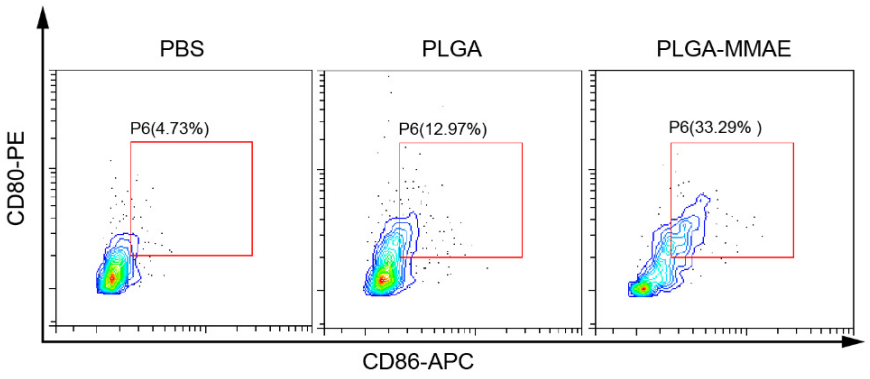

(a)

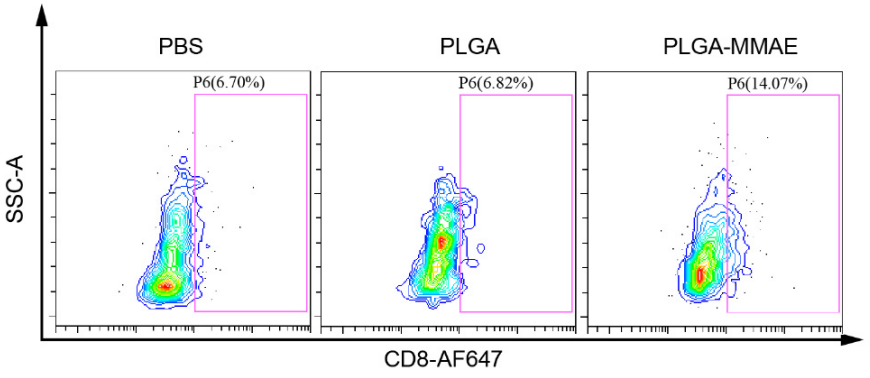

(b)

Fig. 6. Flow cytometry analysis of the *in vivo* immune mechanism of PLGA-MMAE treatment. (a) Percentage of CD80 and CD86 expression in $CD45^+$ $CD11C^+$ DCs, $n = 3$ mice per group. (b) Proportion of $CD3^+$ $CD8^+$ T cells in $CD45^+$ T cells among different treatment groups, $n = 3$ mice per group. (c) Percentage of $CD80^+$ $CD86^+$ in $CD11c^+$ cells among different treatment groups, $n = 3$ mice per group. (d) Proportion of $CD3^+$ $CD8^+$ T cells in $CD45^+$ T cells among different treatment groups, $n = 3$ mice per group. Results are presented as mean ± SD. $^{****}P < 0.001$, $^{***}P < 0.001$, $^{**}P < 0.01$, $^{*}P < 0.05$.

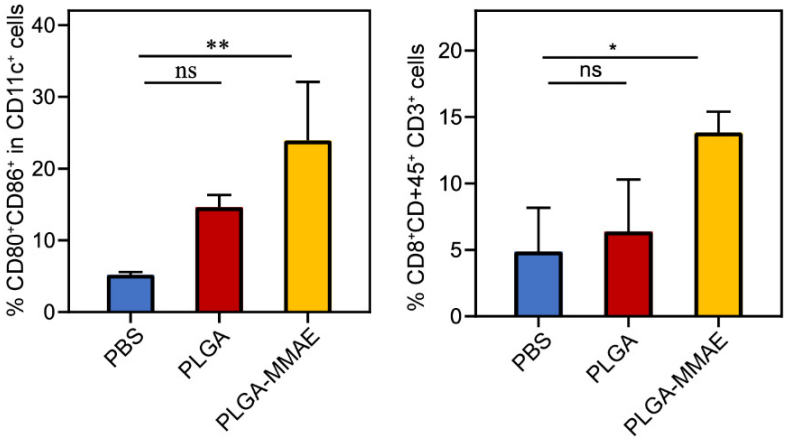

(c) (d)

Fig. 6. (*Continued*)

4. Discussion

Cancer is the main cause of human death and one of the most concerning major health problems in the world.[3,44] Continuous efforts and attempts have been made to explore new cancer treatments. Dolastatin 10 is a marine peptide isolated from the mollusk Dolabella Auricularia. It inhibits tumor growth by acting on tubulin, and its activity is approximately 1000 times greater than that of traditional chemotherapeutic drugs.[7,8] Among them, monomethyl auristatin E (MMAE) is one of the derivatives of marine peptide Dolastatin 10. It exerts its activity through different mechanisms such as inhibiting microtubule polymerization in G2/M phase and blocking cell division or apoptosis, consequently inhibiting tumor growth.[12,14] However, MMAE cannot be used as a single antitumor drug because of its high cytotoxicity. When killing tumor cells, MMAE also causes an extensive damage to normal cells, causing serious toxic side effects. Therefore, the improvement of the bioavailability of MMAE is crucial for an effective treatment.

In this paper, the use of PLGA-b-PEG_{2000} loading MMAE increased its bioavailability in tumor therapy *in vivo*. PLGA have been widely used in many fields, including for a controllable drug release, tissue engineering, and regenerative medicine.[28,29] Previous studies showed that PLGA is a biodegradable polymer, which breaks down into small molecules (lactic acid and glycolic acid) when degraded *in vivo*.[30] Thus, PLGA was chosen as a nanocarrier for an effective delivery of MMAE. In addition, PEG was covalently bound to the PLGA to increase drug accumulation at the tumor site, inhibit tumor growth, and reduce the toxic effect of MMAE on normal cells. Moreover, PLGA-MMAE demonstrated a high MMAE drug loading rate (78.7%), as well as good stability at both 4°C and 37°C (Fig. 1).

The study revealed a notably reduced cytotoxicity of PLGA-MMAE compared to free MMAE, even when both were administered at equivalent concentrations. PLGA-MMAE significantly reduced the toxicity of MMAE, with an IC50 value of 430 nM, which was approximately 40 times higher than that of free MMAE. The cytotoxic effect of PLGA-MMAE gradually increased with the extension of the incubation time since MMAE was released from PLGA-MMAE. PLGA-MMAE NPs had the capacity of a sustained release of MMAE exerting a cytotoxic effect on 4T1 cells in a dose- and time-dependent manner. Besides the strong cytotoxic effect, free MMAE caused ICD, which triggered the antitumor immune response by exposing CRT to the cell membrane surface and HMGB1.[39,45] The immunofluorescence staining images showed that PLGA-MMAE also caused ICD *in vitro*, which was beneficial for the activation of the immune response *in vivo* (Fig. 2). Furthermore, PLGA-MMAE effectively accumulated in the tumor through the EPR effect *in vivo* (Fig. 3). The PLGA-MMAE used in the 4T1 model showed a

significantly improved survival rate compared to that of free MMAE, which confirmed its substantially improved therapeutic effect *in vivo* (Fig. 4). H&E and biochemical analysis (Fig. 5) revealed that free MMAE induced severe systemic cytotoxic side effects at a dose of 4 mg/kg, but no systemic toxic side effects occurred in the PLGA-MMAE group, confirming that PLGA-MMAE had superior biocompatibility *in vivo*. Additionally, PLGA-MMAE treatment promoted DC maturation and $CD8^+$ T cell infiltration in the tumor (Fig. 6). It might be attributed to the continuous release of MMAE in the tumor by PLGA-MMAE, causing tumor cell apoptosis and further induction of a stronger immune response by ICD effect. Therefore, the modification of PLGA as a nanocarrier with tumor-specific antigenic peptides or antibody fragments needs further exploration to obtain the best therapeutic effect of MMAE.

5. Conclusions

In this paper, PLGA-MMAE was successfully prepared and characterized, showing reduced toxicity and improved biocompatibility of MMAE compared with free MMAE. *In vitro* experiments confirmed the sustained release and ICD effects of PLGA-MMAE nanoparticles. Notably, PLGA-MMAE has sustained-release properties, which not only improve the biosafety of MMAE, but also inhibit tumor growth. Furthermore, PLGA-MMAE exhibited the ability to induce cell apoptosis and elicit a certain level of immune response for cancer treatment. Overall, this study offers a secure and effective chemotherapy approach, along with a straightforward synthetic process for MMAE-based nanoparticles. Consequently, this study holds promising implications for improving cancer therapies and underscores the potential for safer and more impactful treatments in the future.

Acknowledgments

This research was funded by the Hainan Provincial Joint Project of Sanya Yazhou Bay Science and Technology City (No. 820LH027), the Hainan Provincial Natural Science Foundation of China (No. 823RC472), the Open Project Program of Wuhan National Laboratory for Optoelectronics (No. 2021WNLOKF008), the Hainan University Scientific Research Foundation (KYQD(ZR)-19107). The animal study protocol was approved by the ethics committee of Hainan University. We thank the Hainan University School of Biomedical Engineering for the support in data acquisition, and the Analytical & Testing Center of Hainan University for high performance liquid chromatography measurements. Changqiang Xie and Yan Wang contributed equally to this work.

Conflicts of Interest

The authors declare that there are no conflicts of interest relevant to this article.

Appendix

The following supporting information can be submitted to MDPI along with the manuscript, Figure S1: Standard curve of RP-HPLC external standard method for PLGA-MMAE nanoparticles. (a) The peak area of MMAE was plotted against its concentration in the standard solutions. (b) The linear regression equation and the correlation coefficient (R^2) are shown. Figure S2: Cell viability of MC38 cells (a) and Panc02-H7 (b) cells and treated with PLGA-MMAE and free MMAE at different concentrations (0–1000 nM) for 24 h evaluated by CCK-8 assay. Results are presented as mean ± SD, $n = 3$. Figure S3: Gating strategy for the analysis of DCs and functional molecules in within tumor tissue. Figure S4: Gating strategy for the analysis of immune T cells and functional molecules in within tumor tissue.

Supplementary Materials

The Supplementary Materials are available at: https://www. worldscientific.com/doi/suppl/10.1142/S1793545823500244.

References

1. A. R. Carroll, B. R. Copp, R. A. Davis, R. A. Keyzers, M. R. Prinsep, "Marine natural products," *Nat. Prod. Rep.* **37**(2), 175–223 (2020).
2. J. W. Blunt, A. R. Carroll, B. R. Copp, R. A. Davis, R. A. Keyzers, M. R. Prinsep, "Marine natural products," *Nat. Prod. Rep.* **35**(1), 8–53 (2018).
3. D. Matulja, F. Vranješević, M. Kolympadi Markovic, S. K. Pavelić, D. Marković, "Anticancer activities of

marine-derived phenolic compounds and their derivatives," *Molecules.* **27**(4), 1449 (2022).
4. B. Madio, G. F. King, E. A. Undheim, "Sea anemone toxins: A structural overview," *Mar. Drugs.* **17**(6), 325 (2019).
5. F. Cárdenas, M. Thormann, M. Feliz, J. M. Caba, P. Lloyd-Williams, E. Giralt, "Conformational analysis of dehydrodidemnin B (aplidine) by NMR spectroscopy and molecular mechanics/dynamics calculations," *J. Org. Chem.* **66**(13), 4580–4584 (2001).
6. L. Hosta, M. Pla-Roca, J. Arbiol, C. López-Iglesias, J. Samitier, L. J. Cruz, M. J. Kogan, F. Albericio, "Conjugation of Kahalalide F with gold nanoparticles to enhance *in vitro* antitumoral activity," *Bioconjug. Chem.* **20**(1), 138–146 (2009).
7. G. Gao, Y. Wang, H. Hua, D. Li, C. Tang, "Marine antitumor peptide dolastatin 10: Biological activity, structural modification and synthetic chemistry," *Mar. Drugs.* **19**(7), 363 (2021).
8. N. Lopes, M. B. Pacheco, D. Soares-Fernandes, M. P. Correia, V. Camilo, R. Henrique, C. Jerónimo, "Hydralazine and enzalutamide: Synergistic partners against prostate cancer," *Biomedicines* **9**(8), 976 (2021).
9. K. W. Yeoh, A. Prawira, M. Z. Saad, K. M. Lee, E. M. Lee, G. K. Low, M. Mohd Nasir, HB., J. H. Phua, W. W. Chow, I. J. Lim, Y. B. Omar, R. Z. Ho, T. B. Le, T. C. Vu, K. C. Soo, H. Huynh, "Vinorelbine augments radiotherapy in hepatocellular carcinoma," *Cancers* **12**(4), 872 (2020).
10. J. Zhang, L. G. Hansen, O. Gudich, K. Viehrig, L. M. Lassen, L. Schrübbers, K. B. Adhikari, P. Rubaszka, E. Carrasquer-Alvarez, L. Chen, V. D'Ambrosio, B. Lehka, A. K. Haidar, S. Nallapareddy, K. Giannakou, M. Laloux, D. Arsovska, M. A. Jørgensen, L. J. Chan, M. Kristensen, H. B. Christensen, "A microbial supply chain for production of the anti-cancer drug vinblastine," *Nature* **609** (7926), 341–347 (2022).
11. Y. Wang, J. Yu, D. Li, L. Zhao, B. Sun, J. Q. Wang, Z. Wang, S. Zhou, M. Wang, Y. Yang, H. X. Liu, H. Zhang, Q. Lv, Q. Jiang, Z. He, Y. Wang, "Paclitaxel derivative-based liposomal nanoplatform for potentiated chemo-immunotherapy," *J Control Release* **341**, 812–827 (2022).
12. J. A. Francisco, C. G. Cerveny, D. L. Meyer, B. J. Mixan, K. Klussman, D. F. Chace, S. X. Rejniak, K. A. Gordon, R. DeBlanc, B. E. Toki, C. L. Law, S. O. Doronina, C. B. Siegall, P. D. Senter, A. F. Wahl, "cAC10-vcMMAE, an anti-CD30-monomethyl auristatin E conjugate with potent and selective antitumor activity," *Blood* **102**(4), 1458–1465 (2003).
13. D. Dornan, F. Bennett, Y. Chen, M. Dennis, D. Eaton, K. Elkins, D. French, M. A. Go, A. Jack, J. R. Junutula, H. Koeppen, J. Lau, J. McBride, A. Rawstron, X. L. Shi, N. Yu, S. F. Yu, P. Yue, B. Zheng, A. Ebens, A. G. Polson, "Therapeutic potential of an anti-CD79b antibody-drug conjugate, anti-CD79b-vc-MMAE, for the treatment of non-Hodgkin lymphoma," *Blood* **114**(13), 2721–2729 (2009).
14. S. M. Kyu, S. Yang, I. Sun, K. Y. Kim, "Tumor-activated carrier-free prodrug nanoparticles for targeted cancer Immunotherapy: Preclinical evidence for safe and effective drug delivery," *Adv. Drug Deliv. Rev.* **183**, 114177 (2022).
15. A. G. Polson, J. Calemine-Fenaux, P. Chan, W. Chang, E. Christensen, S. Clark, F. J. de Sauvage, D. Eaton, K. Elkins, J. M. Elliott, G. Frantz, R. N. Fuji, A. Gray, K. Harden, G. S. Ingle, N. M. Kljavin, H. Koeppen, C. Nelson, S. Prabhu, H. Raab, S. Ross, "Antibody-drug conjugates for the treatment of non-Hodgkin's lymphoma: Target and linker-drug selection," *Cancer Res.* **69**(6), 2358–2364 (2009).
16. M. A. Fanale, "Brentuximab vedotin for advanced Hodgkin's lymphoma," *Lancet Oncol.* **18**(12), 1566–1568 (2017).
17. D. S. Hong, O. S. Tehrani, H. Safran, C. E. Steuer, J. Lacy, M. H. Taylor, T. J. George, R. A. Rangwala, S. Jain, L. V. Nicacio, M. T. Cho, "SGNTV-001: Open label phase 2 study of tisotumab vedotin for locally advanced or metastatic disease in solid tumors," *J. Clin. Oncol.* **37**(15), 3160–3160 (2019).
18. X. Sheng, Z. He, Y. Shi, H. Luo, W. Han, X. Yao, B. Shi, J. Liu, C. Hu, Z. Liu, H. Guo, G. Yu, Z. Ji, S. Yu, Y. Hu, J. Guo, J. Ying, J. Fang, A. Zhou, J. Guo, "RC48-ADC for metastatic urothelial carcinoma with HER2-positive: Combined analysis of RC48-C005 and RC48-C009 trials," *J. Clin. Oncol.* **40**(16), 4520–4520 (2022).
19. M. Alt, C. Stecca, S. Tobin, D. Jiang, S. S. Sridhar, "Enfortumab Vedotin in urothelial cancer," *Ther. Adv. Urol.* **12**, 1756287220980192 (2020).
20. E. D. Deeks, "Polatuzumab vedotin: First global approval," *Drugs* **79**(13), 1467–1475 (2019).
21. A. B. Hill, M. Chen, C. Chen, B. A. Pfeifer, C. H. Jones, "Overcoming gene-delivery hurdles: Physiological considerations for nonviral vectors," *Trends Biotechnol.* **34**(2), 91–105 (2016).
22. H. J. Kim, A. Kim, K. Miyata, K. Kataoka, "Recent progress in development of siRNA delivery vehicles for cancer therapy," *Adv. Drug Deliv. Rev.* **104**, 61–77 (2016).
23. Z. Zhao, A. Ukidve, J. Kim, S. Mitragotri, "Targeting strategies for tissue-specific drug delivery," *Cell* **181**(1), 151–167 (2020).
24. R. L. Best, N. E. LaPointe, O. Azarenko, H. Miller, C. Genualdi, S. Chih, B. Shen, M. A. Jordan,

L. Wilson, S. C. Feinstein, N. J. Stagg, "Microtubule and tubulin binding and regulation of microtubule dynamics by the antibody drug conjugate (ADC) payload, monomethyl auristatin E (MMAE): Mechanistic insights into MMAE ADC peripheral neuropathy," *Toxicol. Appl. Pharmacol.* **421**, 115534 (2021).
25. J. C. Masters, D. J. Nickens, D. Xuan, R. L. Shazer, M. Amantea, "Clinical toxicity of antibody drug conjugates: A meta-analysis of payloads," *Invest New Drugs* **36**(1), 121–135 (2018).
26. B. A. Teicher, R. V. J. Chari, "Antibody conjugate therapeutics: Challenges and potential," *Clin. Cancer Res.* **17**(20), 6389–6397 (2011).
27. P. Khongorzul, C. Ling, F. U. Khan, A. U. Ihsan, J. Zhang, "Antibody-drug conjugates: A comprehensive review," *Mol. Cancer Res.* **18**(1), 3–19 (2020).
28. T. T. Hansel, H. Kropshofer, T. Singer, J. A. Mitchell, A. J. T. George, "The safety and side effects of monoclonal antibodies," *Nat. Rev. Drug Discov.* **9**(4), 325–338 (2010).
29. E. Lagreca, V. Onesto, C. Di Natale, S. La Manna, P. A. Netti, R. Vecchione, "Recent advances in the formulation of PLGA microparticles for controlled drug delivery," *Prog. Biomater.* **9**(4), 153–174 (2020).
30. R. Di Toro, V. Betti, S. Spampinato, "Biocompatibility and integrin-mediated adhesion of human osteoblasts to poly(DL-lactide-co-glycolide) copolymers," *Eur. J. Pharm. Sci.* **21**(2–3), 161–169 (2004).
31. C. Martins, F. Sousa, F. Araújo, B. Sarmento, "Functionalizing PLGA and PLGA derivatives for drug delivery and tissue regeneration applications," *Adv. Healthc. Mater.* **7**(1), 1701035 (2018).
32. P. Gentile, V. Chiono, I. Carmagnola, P. V. Hatton, "An overview of poly(lactic-co-glycolic) acid (PLGA)-based biomaterials for bone tissue engineering," *Int. J. Mol. Sci.* **15**(3), 3640–3659 (2014).
33. A. L. Silva, R. A. Rosalia, E. Varypataki, S. Sibuea, F. Ossendorp, W. Jiskoot, "Poly-(lactic-co-glycolic-acid)-based particulate vaccines: Particle uptake by dendritic cells is a key parameter for immune activation," *Vaccine* **33**(7), 847–854 (2015).
34. X. Weng, Z. Bao, X. Wei, "Binary organic nanoparticles with enhanced reactive oxygen species generation capability for photodynamic therapy," *J. Innov. Opt. Health Sci.* **14**(3), 2150009 (2021).
35. A. Kumari, S. K. Yadav, S. C. Yadav, "Biodegradable polymeric nanoparticles based drug delivery systems," *Colloids Surf. B.* **75**(1), 1–18 (2010).
36. F. Danhier, E. Ansorena, J. M. Silva, R. Coco, B. A. Le, V. Préat, "PLGA-based nanoparticles: An overview of biomedical applications," *J. Control Release.* **161**(2), 505–522 (2012).
37. S. Wilhelm, A. J. Tavares, Q. Dai, S. Ohta, J. Audet, H. F. Dvorak, W. C. W. Chan, "Analysis of nanoparticle delivery to tumours," *Nat. Rev. Mater.* **1**(5), 16014 (2016).
38. J. Fucikova, O. Kepp, L. Kasikova, G. Petroni, T. Yamazaki, P. Liu, L. Zhao, R. Spisek, G. Kroemer, L. Galluzzi, "Detection of immunogenic cell death and its relevance for cancer therapy," *Cell Death Dis.* **11**(11), 1013 (2020).
39. X. Xiong, J. Zhao, R. Su, C. Liu, X. Guo, S. Zhou, "Double enhancement of immunogenic cell death and antigen presentation for cancer immunotherapy," *Nano Today* **39**, 101225 (2021).
40. F. Zhou, X. Li, S. Song, J. T. Acquaviva III, R. F. Wolf, E. W. Howard, W. R. Chen, "Anti-tumor responses induced by laser irradiation and immunological stimulation using a mouse mammary tumor model," *J. Innov. Opt. Health Sci.* **6**(4), 1350039 (2013).
41. S. J. Park, W. D. Ye, R. Xiao, C. Silvin, M. Padget, J. W. Hodge, C. Van Waes, N. C. Schmitt, "Cisplatin and oxaliplatin induce similar immunogenic changes in preclinical models of head and neck cancer," *Oral Oncol.* **95**, 127–135 (2019).
42. T. D. Mckee, J. Chen, I. Corbin, G. Zheng, R. Khokha, "Quantifying nanoparticle transport in vivo using hyperspectral imaging with a dorsal skinfold window chamber," *J. Innov. Opt. Health Sci.* **5**(4), 1250023 (2012).
43. R. Han, Q. Liu, Y. Lu, J. Peng, M. Pan, G. Wang, W. Chen, Y. Xiao, C. Yang, Z. Qian, "Tumor microenvironment-responsive Ag2S-PAsp(DOX)-cRGD nanoparticles-mediated photochemotherapy enhances the immune response to tumor therapy," *Biomaterials* **281**, 121328 (2022).
44. C.-W. Chen, T. R. Blackwell, R. Naphas, P. Winnard, V. Raman, K. Glunde, Y. Chen, "Development of needle-based microendoscopy for fluorescence molecular imaging of breast tumor models," *J. Innov. Opt. Health Sci.* **2**(4), 343–352 (2009).
45. S. Long, Y. Zhao, Y. Xu, H. Li, H. Zhao, D. Chen, J. Zeng, H. Qiu, X. Li, Y. Gu, "Immune response induced by hematoporphyrin derivatives mediated photodynamic therapy: Immunogenic cell death and elevated costimulatory molecules," *J. Innov. Opt. Health Sci.* **15**(4), 2240002 (2022).